Измењено: 2023-11-20 09:57:16

Дигитални репозиторијум Рударско-геолошког факултета Универзитета у Београду

[ДР РГФ]

| | | | | |

http://dr.rgf.bg.ac.rs/s/repo/item/0008385

Дигитални репозиторијум Рударско-геолошког факултета Универзитета у Београду омогућава приступ издањима Факултета и радовима запослених доступним у слободном приступу. - Претрага репозиторијума доступна је на www.dr.rgf.bg.ac.rs

The Digital repository of The University of Belgrade Faculty of Mining and Geology archives faculty publications available in open access, as well as the employees' publications. - The Repository is available at: www.dr.rgf.bg.ac.rs

Ore Geology Reviews 163 (2023) 105775

Contents lists available at ScienceDirect

Ore Geology Reviews

journal homepage: www.elsevier.com/locate/oregeorev

Punctuated, episodic magmatism and mineralization of the Rogozna skarn-hosted Au-Zn-Pb-Cu deposits revealed through high-precision U-Pb zircon geochronology

Sean P. Gaynor [a,b,*], Milorad D. Antić [c], Vladica Cvetković [d], Kristina Šarić [d], Urs Schaltegger [a]

[a] Department of Earth Sciences, University of Geneva, 1205 Geneva, Switzerland
[b] Department of Geosciences, Princeton University, Guyot Hall, NJ 08544, USA
[c] Zlatna Reka Resources, Belgrade, Serbia
[d] University of Belgrade, Faculty of Mining and Geology, Belgrade, Serbia

ARTICLE INFO

Keywords:
Skarn mineralization
Magmatic-hydrothermal systems
Subvolcanic intrusions
Zircon geochronology
CA-ID-TIMS

ABSTRACT

The subvolcanic regions of magmatic centers are commonly associated with alteration, mineralization, and economic ore deposits, however the duration and frequency of mineralizing pulses within the overall lifespan of these centers can be poorly defined. Therefore, models for the formation of mineral systems require more high-precision geochronology data to refine their evolutionary models. Rogozna Mountain and its eponymous magmatic complex, located in SW Serbia, hosts multiple base metal deposits associated with variable rock types and structural expressions and serves as a natural laboratory to test the span and periodicity of mineralizing events. Unlike many deposits within the Rogozna magmatic complex (RMC) and elsewhere within the broader Serbo-Macedonian magmatic and metallogenic belt represented by Pb-dominated base metal sulfides, the Rogozna mining project (composed of the Gradina, Medenovac, Copper Canyon and Šanac deposits) also hosts Au-Cu mineralization. Based on previous isotope geochemistry, a single magmatic source was responsible for the sulfide crystallization associated with Au-Cu mineralization at the Copper Canyon deposit. Therefore, a detailed determination of igneous events and their temporal relationship remains crucial for understanding the formation of the Rogozna mineralized system and its multiple deposits.

High-precision chemical abrasion-isotope dilution-thermal ionization mass spectrometry (CA-ID-TIMS) U-Pb zircon geochronology of six representative samples revealed the first phase of oxidized Au-Zn mineralization at the Medenovac deposit occurred prior to 28.833 ± 0.154 Ma, based on the inclusion of mineralized skarn clasts in breccia supported by an igneous-matrix. This age indicates that mineralization and skarn formation began over 1 Myr prior to reduced Au-Cu mineralization at the Copper Canyon deposit, which occurred over a period from approximately 27.76–27.61 Ma associated with a series of texturally diverse but compositionally similar quartz latite intrusions. Trachyandesitic dykes emplaced at 25.384 ± 0.068 Ma represent the youngest igneous event in the RMC. Previous models of the formation of the Rogozna mineralized system are likely flawed by inaccurate unit classification and incomplete sampling of intrusions associated with the deposits, resulting in an unrealistically simplistic evolutionary model for mineralization, rather than a protracted history of episodic alteration and mineralization. Therefore, a reinterpreted temporal hierarchy of the RMC is proposed based on new compositional and geochronological data, defining multiple mineralization events. This work highlights the necessity of combining a robust suite of textural analyses, field relationships, and high-precision geochronology to make accurate interpretations of deposit formation.

1. Introduction

Volcanic-plutonic complexes can contain all the necessary ingredients to form mineral systems during their formation and evolution, due to their ability to introduce fluids, volatiles, metals and heat into the upper crust (e.g., Sillitoe, 2010; Groves et al., 2022). The overall lifespans of these systems can range up to 10 s of Ma (e.g., Dungan et al., 2001; Correa et al., 2016; Gaynor et al., 2019a), and these durations and

* Corresponding author at: Department of Earth Sciences, University of Geneva, 1205 Geneva, Switzerland.
E-mail address: sean.gaynor@princeton.edu (S.P. Gaynor).

https://doi.org/10.1016/j.oregeorev.2023.105775
Received 30 December 2022; Received in revised form 30 October 2023; Accepted 5 November 2023
Available online 7 November 2023
0169-1368/© 2023 The Authors. Published by Elsevier B.V. This is an open access article under the CC BY license (http://creativecommons.org/licenses/by/4.0/).

the lifespans of individual magma bodies within these systems have been interpreted as a critical factor in enrichment of mineralization to reach economic grades (e.g., Chiaradia et al., 2009; Velador et al., 2010; Schöpa et al., 2017). Temporally discrete changes in styles of mineralization and shifts between barren and mineralizing magmatism have been observed in many metallogenic belts, where long-lived, pulsed magmatism reflects distinct changes in tectonic and magmatic conditions that drive magmatic-hydrothermal mineralization (e.g., Zimmerman et al., 2008; Moritz et al., 2016; Rosera et al., 2021; Gaynor et al., 2023). Therefore, developing accurate mineral system models is dependent on detailed, accurate geochronology of the igneous systems associated with mineralization.

The Rogozna magmatic complex (RMC), located at Rogozna Mountain in SW Serbia, contains multiple Pb-dominated, base metal deposits hosted by a diverse suite of country rocks and structures, and these deposits have been interpreted to be the result of mineralization from subvolcanic intrusions (Figs. 1-3; e.g., Janković, 1995; Heinrich and Neubauer, 2002; Borojević-Šoštarić et al., 2011; Borojević-Šoštarić et al., 2013). The deposits at RMC are part of the Kopaonik district, a segment of the Serbo-Macedonian metallogenic province spanning the central Balkan peninsula along a NNW trend (e.g., Janković, 1990, Jelenković, et al., 2008). The Kopaonik metallogenic district predominantly includes post-Eocene base metal skarn- or replacement deposits with lenticular and vein ore bodies (e.g., Janković, 1990, 1995). Deposits of the RMC have been mined for Pb and Ag since at least medieval times (Janković, 1990). Following initial exploration and exploitation, these ore deposits have retained the interest of contemporary exploration. Over the years, a suite of analytical methods has been applied on rocks from this area to better understand the geological framework and the interplay of igneous pulses and ore forming processes. However, many of these studies utilized lower precision techniques or employed geochronometers susceptible to resetting during subsequent thermal or hydrothermal events, such as $^{40}K/^{40}Ar$ or $^{40}Ar/^{39}Ar$. As a result, these incremental studies have yet to fully unravel the complexity of deposit formation in this area and did not sample the full range of igneous units present within the RMC.

The Rogozna mineral system, which encompasses the Gradina, Medenovac, Copper Canyon (aka Karavansalija) and Šanac deposits, hosts base metal mineralization similar to other mines and prospects within the Kopaonik district, however it also contains significant Au-Cu mineralization (Fig. 3; Budinov et al., 2015; Burkhard, 2017). Based on drill core observations and historic reports, the Au-Cu phase of mineralization is cut by the base metal mineralization, and this later episode of mineralization was generated from a single magmatic source of sulfur, based on isotope geochemistry (Budinov et al., 2015). Hence, a detailed determination of igneous events and their temporal relationship is crucial for understanding of the Rogozna mineralized system, the potential for Au-Cu mineral exploration within the RMC and elsewhere within the Kopaonik district, and the origin of different metal expressions. Therefore, we utilized chemical abrasion-isotope dilution-thermal ionization mass spectrometry (CA-ID-TIMS) U-Pb zircon geochronology on recently available sample material to unravel the relationship of magmatism, the Au-Cu mineral system, and potential implications for the later base metal overprint. These results build a better mineral systems model for the formation of ore at the RMC, providing insight into the lifespan of a subvolcanic magma system associated with economic mineralization.

2. Geological setting

The RMC is located at the surface expression of a NW-SE striking thrust of the West Vardar ophiolitic belt over the Drina-Ivanjica thrust sheet of the Adria-derived Dinarides in SW Serbia (e.g., Karamata et al., 1992; Dimitrijević, 1997; Schmid et al., 2020; Fig. 1). This contact formed during the complex subduction and final closure of the Mesozoic Tethys in the central Balkans, followed by the continental collision

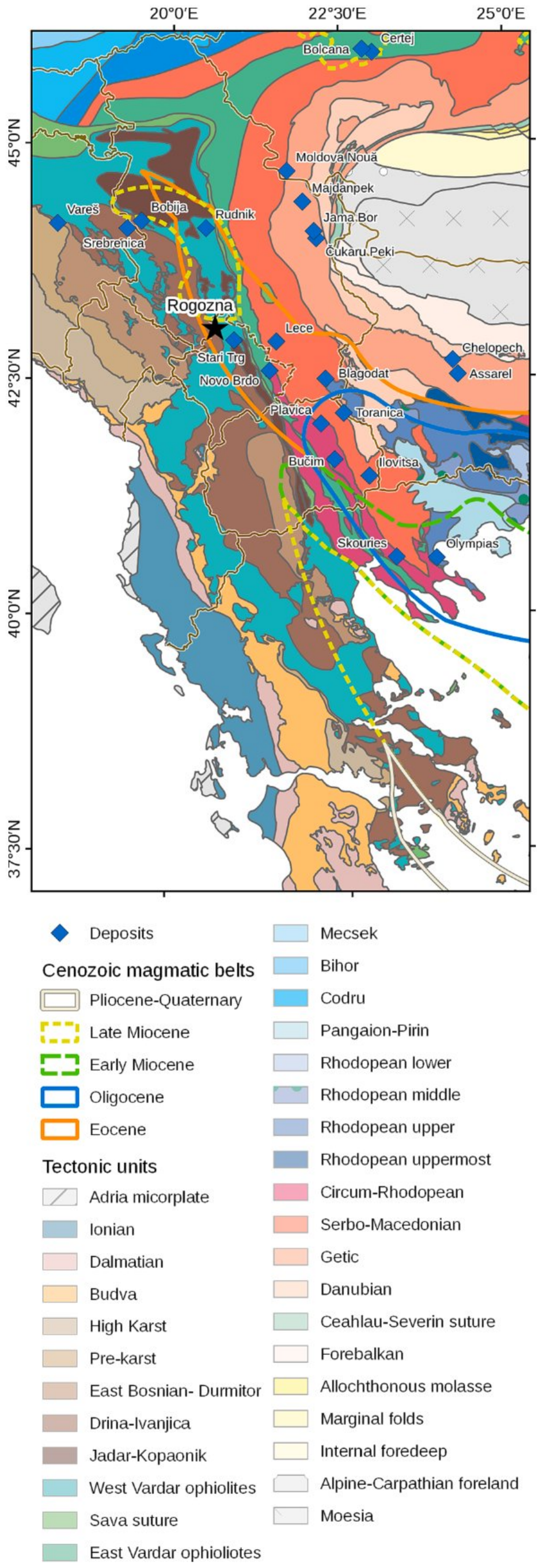

Fig. 1. Tectonic sketch of SE Europe (after Schmid et al., 2020) with extents of the magmatic belts and position of mines and deposits at advanced stage. The position of the Rogozna magmatic complex is indicated with a black star.

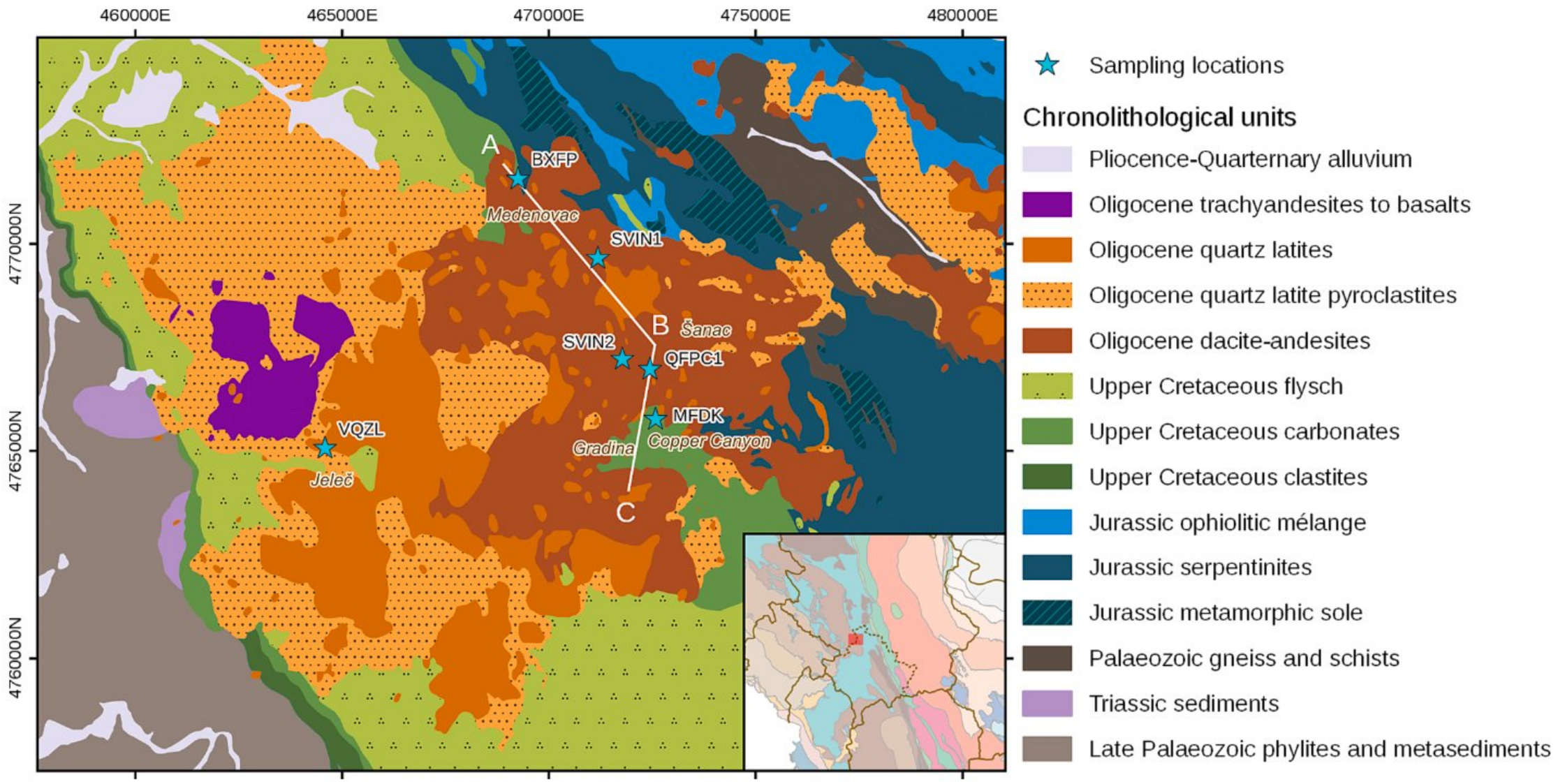

Fig. 2. Simplified geological map of the Rogozna magmatic complex with sample locations for this study (modified from Urošević et al., 1973; Bogdanović, 1982; Karamata et al., 1994; Borojević-Šoštarić et al., 2012). The locations of drill hole samples are given as corresponding drillhole collars. Toponyms and approximate locations of the individual deposits given in brown italics. Line A-B-C shows the map view of the cross section in Fig. 3.

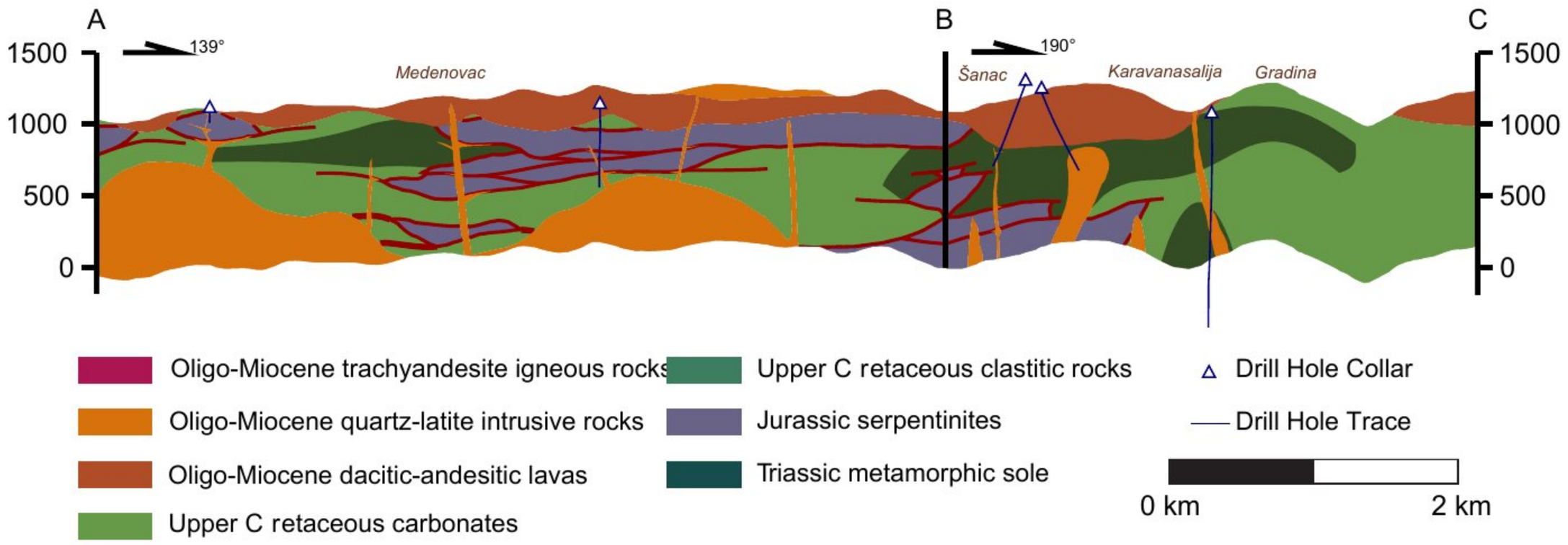

Fig. 3. Simplified cross section of the Rogozna magmatic complex, highlighting the geology of the Medenovac, Gradina and Copper Canyon deposits, along with the drill hole traces of the exploration well used to sample for this study.

between Europe and Adria during the late Mesozoic and earliest Cenozoic (e.g., Karamata, 2006; Schmid et al., 2008; Gallhofer et al., 2015). The Vardar ophiolites are composed of the early Middle Jurassic metamorphic sole and Triassic to Jurassic serpentinized ophiolitic mélange, which were obducted from the Late Jurassic until the earliest Cretaceous (Figs. 1-2; Karamata, 2006 and references therein; Schmid et al., 2008, 2020; Borojević Šoštarić et al., 2014). The eastern footwall of the ophiolitic belt is represented by Paleozoic gneiss and schists of the Jadar-Kopaonik unit and are sporadically exposed at the surface as tectonic windows NE of the RMC (Figs. 2-3; Schmid et al., 2020; Kopaonik block *sensu* Dimitrijević, 1997). The final closure of the Mesozoic Tethys and collision of Adria and Europe in this region is represented by complex imbricated thrusting of the obducted ophiolites and the deposition of Upper Cretaceous clastic sediments up to 50 m thick, bedded limestones and marly carbonates with conglomerate beds up to 200 m thick, and pre-flysch and flysch packages up to 1000 m thick (e.g., Urošević et al., 1973; Dimitrijević, 1997). Both the Drina-Ivanjica unit to the west and the Jadar-Kopaonik unit with overriding ophiolites to the East have been suggested as the detrital sources of the flysch (Urošević et al., 1973). The Drina-Ivanjica unit is represented by Upper Palaeozoic schists, phyllites, and other metasedimentary rocks, overlain by clastic and carbonate sedimentary rocks of the Lower and Middle Triassic (Urošević et al., 1973), whereas the Jadar-Kopaonik unit in this region is composed of Middle Triassic shallow-water carbonate rocks overlain by upper Middle Triassic to Upper Triassic cherty metalimestones and Jurassic hemipelagic limestones and radiolarites (Schefer, 2010).

The RMC is part of the larger Serbo-Macedonian magmatic and metallogenic belt (SMMMB), which formed after the Eocene. This magmatic event has been interpreted to be the result of a transition from

collisional to post-orogenic extension (Fig. 1; Cvetković et al., 2004; Andrić et al., 2018). The SMMMB is represented by compositionally diverse volcanic-plutonic centers composed of calc-alkaline, high-K calc-alkaline, ultrapotassic, and shoshonitic rocks, that formed within discrete periods of approximately 35–31 Ma, 28–24 Ma, 15–12 Ma, and less than 9 Ma (Prelević et al., 2005; Borojević-Šoštarić et al., 2012; Moritz et al., 2014; Baker, 2019). Most of the individual volcanic-plutonic complexes are spatially associated with large-scale Mesozoic thrusts within the Dinarides, and therefore these structures have been interpreted to be a first-order control over Oligocene-Miocene magmatism and associated mineralization (e.g., Karamata et al., 1992). Mineralization within the SMMMB is commonly expressed as Pb-Zn-Ag ± Au deposits, whereas minor Cu-porphyry and Sb-As-Au ± Cu epithermal deposits are also present in the southern part of the region (e.g., Janković , 1990; Janković, 1997; Miletić et al., 1998; Serafimovski et al., 2010).

2.1. Review of the current understanding of igneous and metallogenic evolution of RMC

The RMC is located along a NE-trending belt of Oligocene-Miocene magmatic centers and has been interpreted to have formed over a period of four major magmatic phases (Fig. 1; e.g., Borojević-Šoštarić et al., 2012; Hoerler et al., 2022). The first phase of igneous activity identified at RMC are a suite of dacite-andesite lava flows interpreted to have erupted at 29.343 ± 0.029 Ma and a small volume porphyritic intrusion at 28.964 ± 0.007 Ma, based on U-Pb of the youngest zircon grains analyzed in a recent CA-ID-TIMS study (Hoerler et al., 2022). The following (second) phase of magmatism is a suite of quartz-latite intrusions (e.g., Supplementary Fig. 1), which are shoshonitic in composition and host mineral textures indicative of disequilibrium, such as sieved plagioclase phenocyrsts, dissolution in quartz, and phlogopitized biotite and amphibole grains (Borojević-Šoštarić et al., 2012). Previous amphibole and biotite $^{40}Ar/^{39}Ar$ geochronology suggested that this pulse of magmatism ranged from 29.5 ± 0.1 to 27.3 ± 0.1 Ma, potentially overlapping with the first phase of less potassically-enriched magmatism. However, more recent U-Pb CA-ID-TIMS work has interpreted that these intrusions were emplaced between 27.759 ± 0.013 to 27.615 ± 0.009 Ma, based on the weighted mean ages of the youngest population of zircon dates (Hoerler et al., 2022). These intrusive rocks have been broadly named the "crowded porphyry" unit (Hoerler et al., 2022). A suite of pyroclastic and volcaniclastic rocks exposed in the western part of the RMC have been interpreted as a result of this pulse of magmatism, due to introduction of volatiles during magma mixing (Fig. 2; Karamata et al., 1994; Borojević-Šoštarić et al., 2012). The third phase of magmatism was interpreted to take place at 27.583 ± 0.031 Ma based on the youngest zircon analyzed from a sample of cross cutting granite porphyry, termed "proper porphyry" unit (Hoerler et al., 2022). The final magmatic pulse is a suite of undated high-K calk-alkaline to shoshonitic series basaltic andesites, trachyandesites, trachybasalts and basalts exposed in the western part of RMC (Fig. 2; e.g., Urošević et al., 1973; Karamata et al., 1994; Cvetković et al., 2004; Borojević-Šoštarić et al., 2012).

Within the RMC, Rogozna mining projects are composed of the Gradina (reduced Au + Zn ± Cu), Medenovac (oxidized Zn + Cu + Au), Copper Canyon (reduced Au + Cu) and Šanac (Au + Cu ± Zn ± Bi) deposits, mainly hosted in skarn bodies and to a lesser extent the overlying volcanic rocks, as well as vein hosted epithermal Pb + Ag ± Zn mineralization (Supplementary Fig. 2; e.g., Janković, 1995; Budinov et al., 2015). Extensive prograde skarn formation, dominated by grossular garnet, which occurred largely within Upper Cretaceous marly carbonate rocks and more rarely in the base of the volcanic stack, has been interpreted to be the result of the earliest phases of intrusions within the RMC, and therefore interpreted to occur at 28.964 ± 0.007 Ma (Hoerler et al., 2022). Following this high-temperature skarn-forming event, the skarn was overprinted by a lower-temperature hydrothermal event associated with Cu + Fe + Zn + As + Au ± Bi mineralization at Gradina, Copper Canyon (Budinov et al., 2015) and Šanac deposits. Finally, the emplacement of the quartz-latite "crowded porphyry" dikes further mineralized the system, and have been interpreted as particularly important in enriching Au ± Bi within the system (Burkhard, 2017). This stage of quartz-latitic magmatism was followed by the emplacement of epithermal veins associated with Pb + Ag ± Zn mineralisation (Figure ii). The complexity of alteration assemblages and associated vein systems related to these thermo-chemical events, represented by multiple overprinting cycles that likely occurred in relatively narrow time frames, remain beyond the scope of this article and will be discussed in separate studies. Furthermore, despite the substantial amount of drilling completed to date, current exploration does not fully constrain the ore bodies, hence any assessment of mineralization and alteration associations would be tentative. The final emplacement period of unmineralized and weakly metasomatized "proper porphyries" has been interpreted to be the end of mineralization at RMC (Hoerler et al., 2022).

3. Methods & sample descriptions

To better understand the evolution of the Rogozna mineral system, we sampled six units from RMC (Fig. 2; Table 1), with a goal of sampling the full magmatic history of the igneous systems associated with mineralization, as well as those events pre- and postdating the formation of the mineral system (Figs. 3-5). Samples were predominantly obtained from exploratory drill core with a single sample from a surface exposure. Mineral abbreviations according to Whitney and Evans (2010).

3.1. Optical microscopy

Mineralogical-petrological determinations were obtained using polarized transmitted light microscopy. The procedure of making thin sections included: sample cutting, polishing and gradually thinning of a sample to a thickness of approximately 0.02 mm, which were embedded into Canada-balsam. Analyses were done using a petrographic microscope Leica DMLSP, coupled with a digital camera (type DFC290HD). All images are obtained by software LAS V4.1.

3.2. U-Pb Zircon CA-ID-TIMS geochronology

Samples were jaw-crushed, disc milled, and sieved. Heavy minerals were concentrated using a Wilfley table, then a Frantz electromagnetic separator, and finally by standard heavy liquid (diiodomethane) concentration. Zircon grains from the concentrated materials were then handpicked under a binocular microscope. Once zircon grains had been extracted from the samples, they were annealed in a muffle furnace at 900 °C for 48 h (Mundil et al., 2004). The annealed grains were chemically abraded at 210 °C for 12 h in concentrated HF in 3 ml Savillex beakers placed in a Parr digestion vessel (Mattinson, 2005; Widmann et al., 2019). The grain fragments remaining after chemical abrasion were then leached on a hotplate at 80 °C in 6 N HCL overnight, followed by further cleaning through four rounds of 7 N HNO_3 in combination with ultrasonication. Individual cleaned zircon crystals were then loaded into individual 200 μl Savillex microcapsules, spiked with the EARTHTIME $^{202}Pb + ^{205}Pb + ^{233}U + ^{235}U$ tracer solution (calibration version 3; McLean et al., 2011; Condon et al., 2015) and dissolved with about 70 μl HF and trace HNO_3 in a Parr digestion vessel at 210 °C for at least 48 h. Following dissolution, the samples were dried down and converted to a chloride by placing them back in the oven overnight in 6 N HCl. The samples were then dried down again and re-dissolved in 3 N HCl, and purified to U and Pb through anion exchange column chromatography (Krogh, 1973). Once purified, the U and Pb fractions were combined in cleaned 7 ml Savillex beakers and dried down with trace H_3PO_4, prior to loading on outgassed zone-refined Re ribbon filaments with a Si-gel emitter.

Table 1
Sample descriptions and locations.

Sample name	Prospect	WGS 84[a]		UTM 34N[b]		Gauß-Krüger[c]		Elevation [m asl]	Sample type	Sample length [m]	Description
		Easting	Northing	Easting	Northing	Easting	Northing				
MFDK	Copper Canyon	20.6634	43.04408	472,584	4,765,765	7,473,009	4,766,682	1028	half core	2	Fine grained porphyritic trachyandesitic intrusive
QFPC1	Šanac	20.66165	43.05496	472,446	4,766,974	7,472,872	4,767,891	1201	half core	2	Sericite-carbonate altered crowded porphyritic quartz-latitic intrusive
SVIN2	Šanac	20.65345	43.05712	471,780	4,767,217	7,472,205	4,768,134	1262	half core	2	Propilitised quartz-latitic porphyry intrusive
SVIN1	Medenovac	20.64605	43.079	471,187	4,769,649	7,471,612	4,770,567	1097	half core	2	Slightly altered (propylitic to potassic) porphyritic quartz-latitic intrusive
VQZL	Vojkoviće	20.56527	43.03744	464,587	4,765,064	7,465,010	4,765,981	875	rock chip	1	Groundmass-supported polymictic volcaniclastic breccia
BXFP	Medenovac	20.62222	43.0962	469,255	4,771,567	7,469,680	4,772,486	1065	half core	2	Clast-supported polymict breccia with igneous groundmass

The locations of drillhole samples are given as corresponding drillhole collars.
[a] Geodetic coordinate system in decimal degrees.
[b] Projected coordinate system using WGS84 datum; in metres.
[c] Projected coordinate system used in SFR Yugoslavian basic geological 1:100 000 maps; in metres.

Uranium and lead isotope analyses were completed on an Isotopx Phoenix TIMS machine at the University of Geneva (Switzerland). Lead measurements were made in dynamic mode using a Daly photomultiplier, and U was measured as an oxide in static mode using Faraday cups coupled to 10^{12} Ω resistors. The $^{18}O/^{16}O$ oxygen isotope ratio in uranium oxide was assumed to be 0.00205 based on previous measurements of the U500 standard. Mass fractionation of Pb and U was corrected using the composition of the spike solution (Condon et al., 2015). The abundance of U was calculated using a sample composition $^{238}U/^{235}U$ value of 137.818 ± 0.045 (2σ, Hiess et al., 2012). All common Pb was considered laboratory blank and was corrected using the long-term isotopic composition of the Pb blank at the University of Geneva (Schaltegger et al., 2021). All data were processed with the Tripoli and Redux U–Pb software packages (Bowring et al., 2011; McLean et al., 2011). All ages were corrected for initial ^{230}Th disequilibrium in the melt using a Th/U composition of the magma of 3.5. Earthtime ET100 standard solution analyzed during the period of these analyses yielded a value of 100.177 ± 0.010 Ma (MSWD = 2.6; n = 8), within uncertainty of the recently reported inter-laboratory calibrated value of 100.173 ± 0.003 Ma for this solution (Schaltegger et al., 2021). The uncertainty of U-Pb weighted mean ages are presented in x/y/z notation (analytical error/spike calibration + analytical error/decay constant + spike calibration + analytical error) after Schoene et al. (2006).

4. Results

4.1. Sample petrography

Detailed descriptions of the samples analyzed for CA-ID-TIMS U-Pb geochronology are provided below. Imagery of these samples can also be found in Fig. 4.

4.2. BXFP

Sample BXFP is a subvolcanic, clast-supported polymict breccia with a fine-grained crystalline igneous groundmass supporting the clasts (Figs. 4 and 5). The angular to subangular clasts within the breccia include mineralized skarn with pyrite, chalcopyrite, galena and/or sphalerite, as well as serpentinites and marly limestones. The igneous groundmass is similar to the porphyritic quartz-latite, with a holocrystalline groundmass. Phenocrysts include feldspar and amphibole altered to calcite, chlorite, anhydrite and clay and relatively fresh biotite. Secondary quartz is also present, with opaque minerals oxidized to predominantly iron hydroxide minerals. A split core interval was taken between 21.5 and 23.5 m of hole EOKSC1249 at the Medenovac deposit (assay sample 41249011; Au = 0.69 ppm). This interval of breccia is approximately 30 m thick and is structurally above serpentinite. These breccias have not been dated previously.

4.3. MFDK

Sample MFDK was taken from a dike of fine-grained porphyritic trachyandesite rarely intercepted in the eastern region of the RMC, but more commonly exposed at the surface in the western portion of the RMC (Fig. 2). This unit was sampled from the Copper Canyon deposit, underlying mineralized pyrrhotite skarn. The half core interval was taken between 881 and 884 m of hole EOKSC17101 (assay sample 101438; unmineralized). The dike sampled for this study is approximately 10 m thick. Sample MFDK is a grey to grey-green porphyritic trachyandesite, with somewhat imbricated tabular plagioclase, acicular hornblende and scarce biotite in a hypocrystalline groundmass. It hosts several irregular vesicles that are filled with brown to pink zeolite, but also commonly replaced by a vitreous texture. There are also spherical melt inclusions within the larger plagioclase phenocrysts. Finally, there are fine coronas in amphibole and biotite crystals, indicative of magma mixing during crystallization.

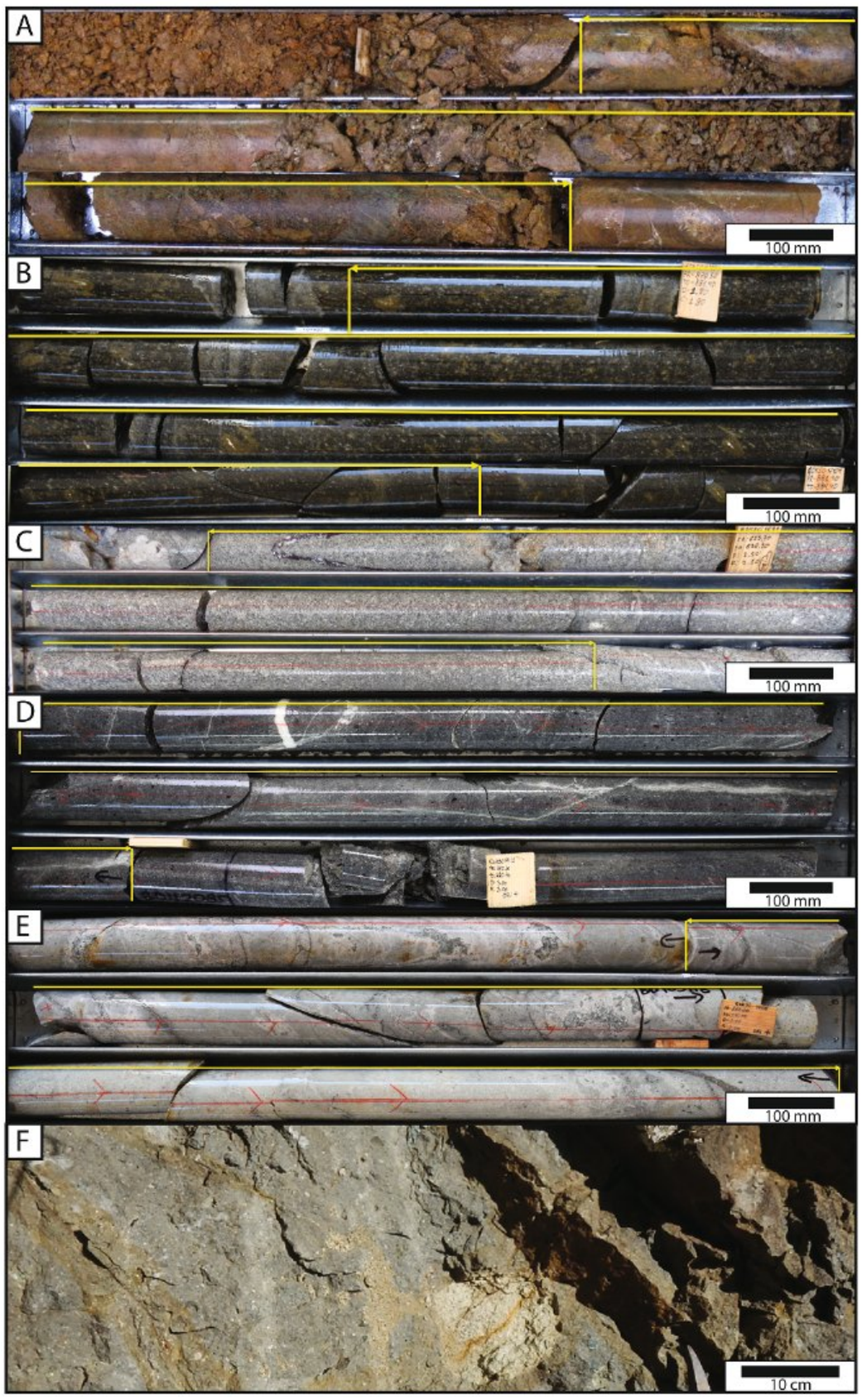

Fig. 4. Representative outcrop and drill core samples for the units dated in this study, including A. BXFP, a subvolcanic clast-supported polymict igneous breccia; B. MFDK, a trachandesite intrusion; C. QFPC1, a quartz latite intrusion; D. SVIN1, an altered porphyritic quartz-latite intrusion; E. SVIN2, an altered porphyritic quartz-latite intrusion; F. VQZL, trachyandesite groundmass-supported polymictic volcaniclastic breccia.

4.4. QFPC1

Sample QFPC1 is sampled from the unit previously logged as the "Crowded Porphyry" and is a white mica-carbonate altered porphyritic quartz-latitic intrusion located in the SW of the Šanac deposit, adjacent to magnetite skarn and underlying the base of the volcanic stack. Previous research sampled a similar unit from the neighboring Copper Canyon deposit, and interpreted to have been emplaced at 27.58 ± 0.03 Ma based on the youngest single CA-ID-TIMS zircon U-Pb date from protracted ages (Hoerler et al., 2022). The "Crowded Porphyry" was collected between 626 and 628 m in hole EOKSC1690 (assay sample 90314; unmineralized). This sample hosts relatively coarse, tabular or slightly elongated plagioclase phenocrysts which are pervasively replaced by fine white mica, calcite and rare anhydrite. These phenocrysts are rarely larger than 4 mm. Rounded or irregular quartz phenocrysts are also approximately as abundant as the plagioclase phenocrysts. Euhedral biotite phenocrysts, up to 4 mm, are commonly replaced by chlorite, anhydrite, and opaque minerals. The groundmass for this sample was likely initially holocrystalline, however, it was subsequently altered, and is now composed of quartz, plagioclase, or secondary adularia. Incipient growth of new biotite was also observed in the groundmass. Assay data from this sample are very similar to other quartz latite intrusions found within the district (Fig. 6; Supplementary Table 1).

Fig. 5. Example drill core of the shallow igneous breccia unit at the base of the volcanic stack, hosting clasts of mineralized skarn set within an igneous-hydrothermal matrix. Image is of drill core EOKSC1678, from the core depth 231.6 to 240.9 m.

4.5. SVIN1

Sample SVIN1 is a propylitically to potassically altered quartz-latite porphyritic intrusive rock with a holocrystalline groundmass. The half core interval was taken between 418 m and 420 m of hole EOKSC17112 in the southern region of the Medenovac deposit (assay sample 112198; minor mineralization, Au = 0.04 ppm). This intrusion is approximately 40 m thick, with serpentinite wall rock. The sample is dark grey, porphyritic, and displays fluidal fabric. Phenocrysts compose approximately 80 % of the sample, and are primarily pale, tabular, and prismatic plagioclase and sanidine up to few millimeters long. Subordinately, there are also smaller and more elongated hornblende and biotite phenocrysts altered into fine aggregates of chlorite, calcite, and gypsum. This rock also contains trace quantities of magnetite and pyrite. Its secondary minerals include quartz, white mica, adularia, and rare new biotite.

4.6. SVIN2

Sample SVIN2 is a quartz-latite porphyry with propylitic alteration, emplaced at the base of an andesitic volcanic suite, and has been mapped as part of the same unit as sample SVIN1. The half core interval was taken between 569 and 571 m of hole EOKSC17105 in the western part of the Šanac deposit (assay sample 105305; minor mineralization, Au = 0.08 ppm). The dike is approximately 15 m thick, intruded beneath the base of the volcanic stack, and is the southernmost occurrence of the SVIN quartz-latite unit. Sample SVIN2 is pale-grey to light brown, with abundant sericitized tabular feldspar phenocrysts up to few mm. Late submillimeter veins with calcite and gypsum overprint the sericitized plagioclase phenocrysts. Mafic minerals are largely replaced by chlorite, calcite, epidote, leucoxene and anhydrite/gypsum. Primary magnetite is also replaced by pyrite. The sample's previously hypocrystalline groundmass shows relics of fluidal fabric and it is partially replaced by clay minerals with secondary quartz and subordinate adularia.

4.7. VQZL

Sample VQZL is a groundmass-supported polymictic volcaniclastic breccia. The sample was collected at a fresh roadside outcrop, north of

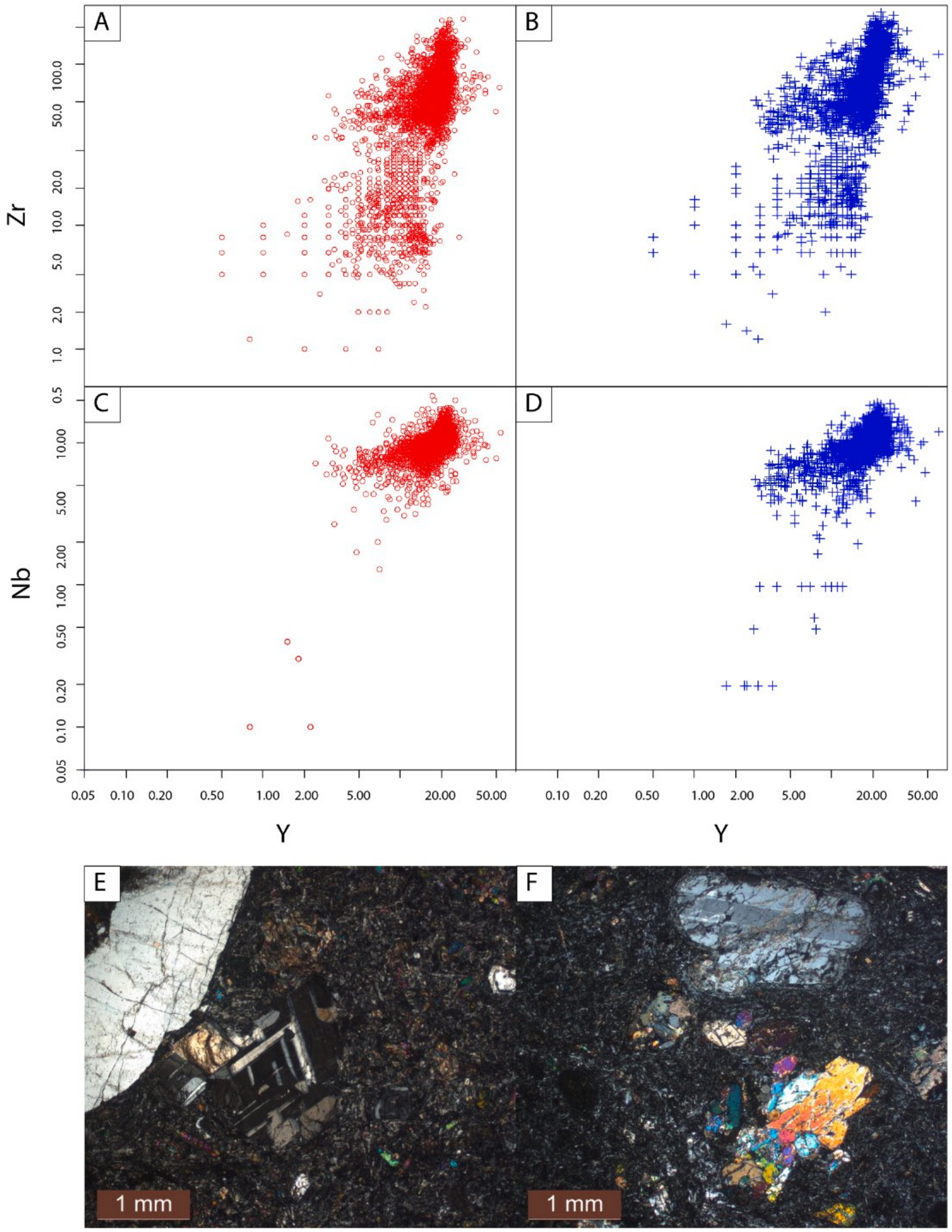

Fig. 6. Comparative Y vs Nb ratios of a) QFPC and b) QFPP; Zr vs Y ratios of c) QFPC and d) QFPP; e) QFPC: Phenocrysts of quartz (Qz) and plagioclase (Pl) set in a holocrystalline groundmass composed of microphenocrysts of plagioclase and epidote as well as of microlites of the same minerals, together with altered amphibole and biotite; cross-polarised light. f) QFPP ZRSD20127 – 420.83 m: A tabular plagioclase phenocryst (Pl), a glomeroporphyritic aggregate of epidote crystals (Ep) and a relict phenocryst of biotite (Bt), enclosed by a fine-grained matrix; cross-polarised light. Data presented in this figure can be found in Supplementary Table 2.

Jeleč hill (Fig. 2). The volcanic clasts are subangular to rounded, up to 20 cm in diameter (mean 2 cm). The majority of the lithic fragments are composed of feldspar-biotite-phyric vesicular quartz-latite. Subordinate fragments include finely porphyritic trachybasalt with phlogopite and replaced olivine phenocrysts. Least abundant clasts include sandstone, marls, and schists.

4.8. Zircon geochronology

Unless otherwise noted, all zircon dates discussed in the text are $^{206}Pb/^{238}U$ dates corrected for initial ^{230}Th disequilibrium, as this chronometer provides the most precise and accurate estimate for rocks of this age (Fig. 7; Supplementary Table 2). The uncertainties for age interpretations are provided in the x/y/z format (analytical error / spike calibration + analytical error / decay constant + spike calibration + analytical error) in order for these ages to be comparable to other studies or different geochronometers; in the text, only x-errors are reported for individual dates.

The samples that yielded the oldest overlapping cluster of Oligocene zircon were from altered quartz-latite porphyritic intrusions. Individual

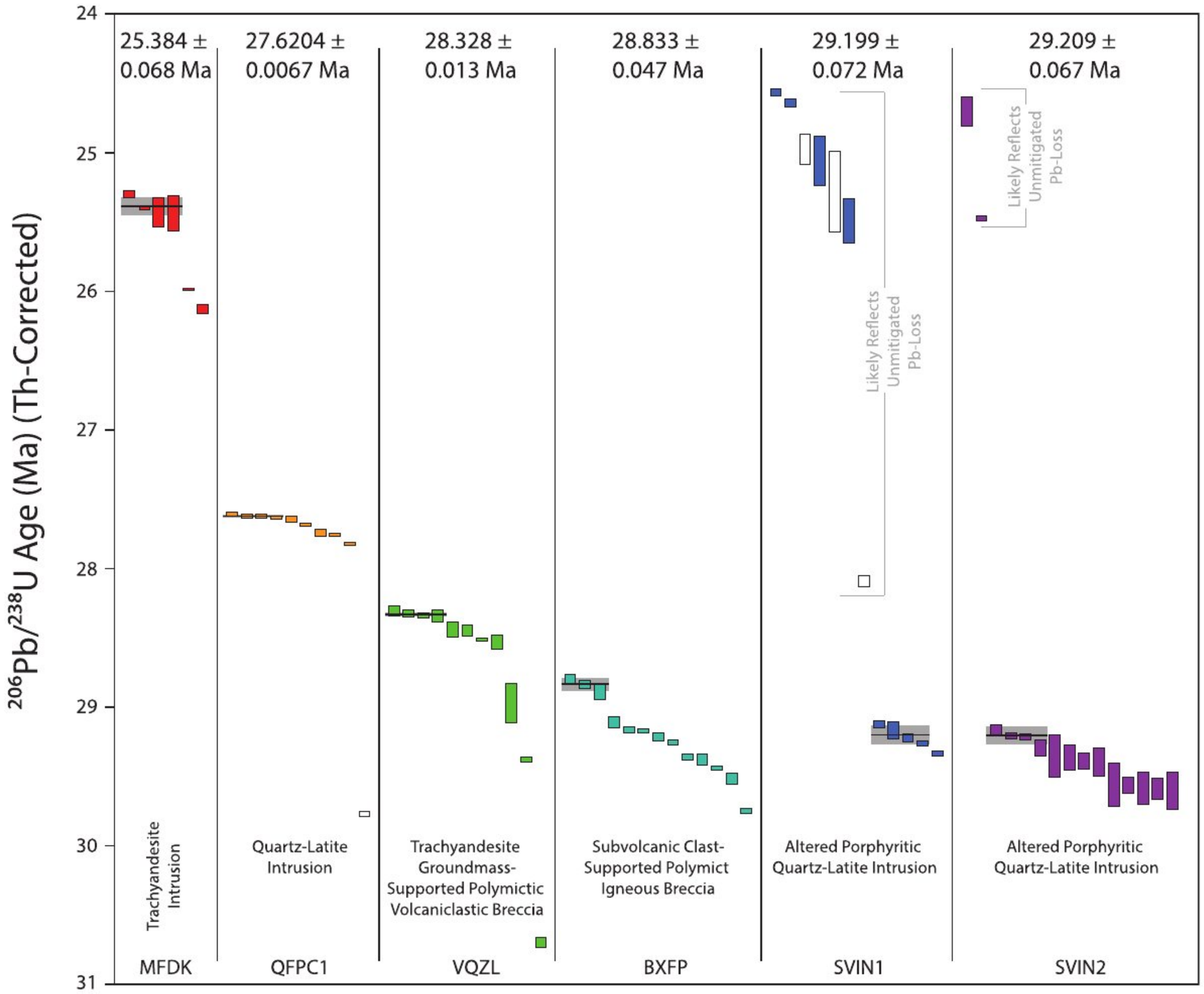

Fig. 7. Rank order plot of Oligocene $^{206}Pb/^{238}U$ CA-ID-TIMS dates for individual zircons from the Rogozna magmatic complex analyzed in this study. Vertical bar height is the 2σ analytical uncertainties for individual analyses. Preferred ages for individual samples are presented as solid black lines, with a gray bar representing the 2σ analytical uncertainty of that interpretation. Multiple older, normally discordant analyses have been omitted from this figure for clarity but are present in Supplementary Table 1 and Supplemental Fig. 3. See text for discussion on age interpretations.

concordant dates from samples of the quartz-latite porphyritic unit range from 24.563 ± 0.025 to 29.331 ± 0.019 Ma in sample SVIN1, and from 24.70 ± 0.11 to 29.61 ± 0.13 Ma for sample SVIN2. Sample SVIN2 also yielded one older, normally discordant analysis with a date of 36.121 ± 0.040. The majority of the age spectra from both samples center on approximately 29 Ma, with non-overlapping, anomalously younger analyses around approximately 25 Ma, and this younger cluster also includes normally discordant analyses.

Individual zircon dates from sample BXFP of a subsurface igneous matrix supported breccia range from 28.799 ± 0.036 to 29.751 ± 0.019 Ma, with minimal age overlap between many of the analyses. All zircon grains analyzed from this sample are concordant within uncertainty. There are three overlapping analyses in the youngest part of the age spectra at approximately 28.8 Ma.

Individual concordant dates from a sample of the surficially exposed groundmass-supported polymictic volcaniclastic breccia (VQZL) range from 28.303 ± 0.036 to 30.699 ± 0.035 Ma, with two older, normally discordant analyses with dates of 43.244 ± 0.019 Ma and 57.695 ± 0.089 Ma. There are four overlapping analyses at the youngest portion of the age spectrum at approximately 28.3 Ma.

Sample QFPC1 of the "crowded porphyry" yielded abundant zircon. Individual concordant dates from this sample range from 27.605 ± 0.016 to 27.821 ± 0.014 Ma, with one older, normally discordant grain with a date of 29.770 ± 0.16 Ma. The majority of the analyzed grains cluster tightly at approximately 27.6 Ma.

Finally, the late trachyandesite intrusions yielded the youngest overlapping cluster of zircon dates in this study. Individual zircon dates from sample MFDK from the porphyritic trachyandesite dike range from 25.300 ± 0.026 to 224.176 ± 0.072 Ma, with a cluster of the youngest ages at approximately 25.4 Ma (n = 4; Supplementary Table 2). All Oligocene dates are concordant within uncertainty (n = 6), while all zircon grains with dates older than Oligocene are normally discordant. All analyses yield an approximately linear relationship in Concordia space, defining an upper intercept of 224.1 ± 2.0 Ma (n = 12; MWSD = 6.7; Supplementary Fig. 3).

5. Discussion

Newly observed field relationships and high-precision U-Pb zircon CA-ID-TIMS geochronology data provide significant insight into the complexity and evolution of magmatism and mineralization at the RMC. Combining these new results with previous data allows for a more complete understanding of the evolution of the mineral system of the RMC, and the lifespan of its individual hydrothermal-magmatic events.

5.1. Geochronological interpretation of obtained results

High-precision geochronology of intrusions associated with ore deposits increasingly yields protracted, complex age spectra, complicated by the variable presence of Pb-loss, antecrysts and xenocrysts (e.g., Tapster et al., 2016; Buret et al., 2017; Li et al., 2017; Gaynor et al., 2019a; Feely et al., 2020; Large et al., 2020, 2021; Rosera et al., 2021;

Ouyang et al., 2023). Age spectra from individual samples in this study have concordant age ranges greater than 1 Myr, far beyond the expected or observed crystallization lifespans of upper crustal magmas and lavas (Fig. 7; e.g., Cathles et al., 1997; Barboni and Schoene, 2014; Gaynor et al., 2019b). Therefore, the full age spectra do not necessarily relate to the emplacement and solidification of the sampled igneous units from RMC and determining emplacement ages for these intrusions requires further interpretation.

Antecrysts and xenocrysts are commonly observed in high-precision data sets, and this has led some studies to interpret the youngest zircon in complicated, high precision age spectra, as reflecting the age of crystallization of a magma or of a volcanic eruption (e.g., Schaltegger et al., 2009; Hoerler et al., 2022). However, in many highly altered or mineralized systems, anomalously young ages are increasingly common in high-precision data sets, in many cases contradicting relative age relationships, and have been interpreted to be the result of incomplete mitigation of Pb-loss during chemical abrasion due to high temperature hydrothermal alteration (e.g., Ovtcharova et al., 2015; Gaynor et al., 2019a; Rosera et al., 2021; Ouyang et al., 2023). Therefore, in this study we interpret that the youngest plateau (or cluster) of concordant ages reflects the final crystallization of a magma, whereas older ages reflect inheritance of xenocrystic or antecrystic material, and anomalously younger ages reflect Pb-loss.

Several of the samples yielded age spectra wherein the youngest cluster of zircon ages define a single statistical population, and in these cases, it is appropriate to calculate a weighted mean age to interpret the final crystallization of those samples. For the breccia sample VQZL, the youngest cluster yields an age of 28.328 ± 0.013/0.015/0.034 Ma (n = 4; MSWD = 1.2) and given the igneous matrix content of this breccia, we interpret that this age reflects formation of the quartz-latitic groundmass. The youngest zircon population from sample QFPC1, the crowded porphyry, yields an age of 27.6204 ± 0.0067/0.009/0.031 Ma (n = 4; MSWD = 1.2), reflecting the final crystallization, and therefore solidification, of this intrusive body.

The age spectra for most other samples in this study are significantly more protracted, and due to the lack of a single statistically relevant cluster of ages, we suggest that simple weighted mean calculations may not accurately reflect a crystallization age. For samples where the youngest overlapping population yields analytical dispersion beyond a single population, we instead calculate weighted mean ages using a suite of overlapping dates, and then use a conservative, larger estimate of uncertainty using half of the difference between the oldest and youngest grains within the overlapping population. This approach has the advantage of ensuring that the age interpreted from a complex zircon spectrum is more likely to be accurate within the presented uncertainty (e.g., Rosera et al., 2021). Sample MFDK likely has significant xenocrystic inheritance, best highlighted by six normally discordant grains which all yielded older $^{206}Pb/^{238}U$ dates. The presence of volumetrically minor xenocrystic inheritance within zircon may not be revealed by CL-imagery and as a result, may be best identified through assessing discordance within high-precision analyses (e.g., Gaynor et al., 2022). The youngest Oligocene population of grains yields significant scatter, and therefore we use the youngest four grains as an estimate for the age of this intrusion. This interpretation yields a $^{206}Pb/^{238}U$ age of 25.384 ± 0.068/0.070/0.084 Ma (n = 4; MSWD = 17), however this interpretation does have the possibility of yielding an inaccurately old age, as it is possible that this cluster of ages still incorporate xenocrystic zircon domains. For sample BXFP, there is significant dispersion within the younger population (MSWD = 4.1), therefore this sample yields an age 28.833 ± 0.047/0.0.049/0.063 Ma, given the more conservative estimate of uncertainty. This age is interpreted to reflect crystallization of the igneous matrix of this breccia sample, and therefore provides a minimum age for the units found as clasts within the breccia.

Finally, both samples of the quartz-latitic dikes at RMC (SVIN1 & SVIN2) have anomalously younger zircon dates, significantly younger than the overall plateau of dates. These samples also have the highest degree of alteration of all samples studied here. We interpret that the anomalously youngest dates reflect open system Pb-loss behavior within select grains, highlighted by the presence of normal discordance in several of the youngest grains in sample SVIN1, and instead interpret that the youngest coherent plateau of zircon ages reflects crystallization and solidification of these intrusions. Given the consistently low abundances of U measured in these crystals and a lack of sufficient time for significant α-decay damage to these crystals, it is unlikely that Pb-loss within these crystals was driven by fast pathway diffusion of Pb due to a metamict crystal structure. Rather, we interpret that zircon from these samples were variably altered by later hydrothermal events, causing partial recrystallization and causing two component mixing between age domains within the zircon. Similar interpretations have been made at other porphyry and skarn deposits, and in those cases the anomalously young zircon ages are also in disagreement with relative age relationships (Gaynor et al., 2019a; Ouyang et al., 2023). This interpretation and using the more conservative approach to estimating uncertainties from scattered data yields an age of 29.199 ± 0.072/0.074/0.090 Ma for SVIN1 and 29.216 ± 0.091/0.093/0.108 Ma for SVIN2. Therefore, these are the oldest rocks analyzed in this study, and both dikes were intruded coevally based on this interpretation (Fig. 7).

5.2. Magmatic Evolution of the Rogozna magmatic complex

These new high-precision geochronology interpretations reveal a more complex magmatic history for RMC than previously identified, and therefore require a revaluation of its formation. Due to the lower precision of existing $^{40}Ar/^{39}Ar$ and K-Ar geochronology datasets, as well as the tendency for these geochronometers to be reset by high temperature and fluid alteration (e.g., Selby and Creaser, 2001; Rosera et al., 2021; Antoine et al., 2022), this interpretation is based largely on the available CA-ID-TIMS U-Pb zircon geochronology datasets. Based on field relationships and the available U-Pb dataset, we divide the magmatic history of the deposit into five periods: (1) early volcanic activity at approximately 29.3 Ma; (2) initial intrusions from 29.2 to 28.8 Ma; (3) intrusion and associated brecciation by trachyandesites (4) emplacement of texturally diverse quartz-latite dikes from 27.8 to 27.6 Ma; (5) the final phase of igneous activity through the intrusion and expulsion of shoshonitic magmas at approximately 25.3 Ma (Figs. 8 and 9). Of these five magmatic periods, only three appear to be directly associated with periods of mineralization and/or alteration.

The first phase is the onset of Oligocene volcanic activity, which was compositionally diverse and ranging from andesite to rhyodacite (e.g., Karamata et al., 1994; Borojević-Šoštarić et al., 2012). These volcanics were previously interpreted to have been emplaced at 29.343 ± 0.03 Ma based on the youngest single CA-ID-TIMS U-Pb zircon age from a sample of rhyodacite within the volcanic stack (Hoerler et al., 2022). This was quickly followed by intrusive magmas from 29.209 ± 0.067 to 28.833 ± 0.097 Ma, which included compositions ranging from quartz-latite (samples SVIN1 and SVIN2) to rhyolite, and produced the earliest known magmatic breccias of the RMC (sample BXFP). It is possible that these two phases overlapped, due to relatively close ages (within 383,000 yr). However, given that the early quartz-latite intrusions cut the base of the volcanic stack and are compositionally and texturally similar to quartz-latite volcanic rocks overlying the voluminous andesite volcanic cover, we interpret that these two units represent different magmatic pulses.

Following a brief quiescence, the third period of Oligocene magmatism at Rogozna is characterized by small volume intrusions of trachyandesite magmas at 28.328 ± 0.013 Ma, which commonly formed the groundmass of subsurface breccias, and likely induced brecciation. This was followed by the more volumetric fourth period of magmatism at the RMC, characterized by the texturally diverse dikes ranging from porphyritic quartz-latite ("crowded porphyry" in Hoerler et al., 2022) to more groundmass dominated textures ("proper porphyry" in Hoerler et al., 2022), and were emplaced between 27.759 ± 0.013 to 27.583 ±

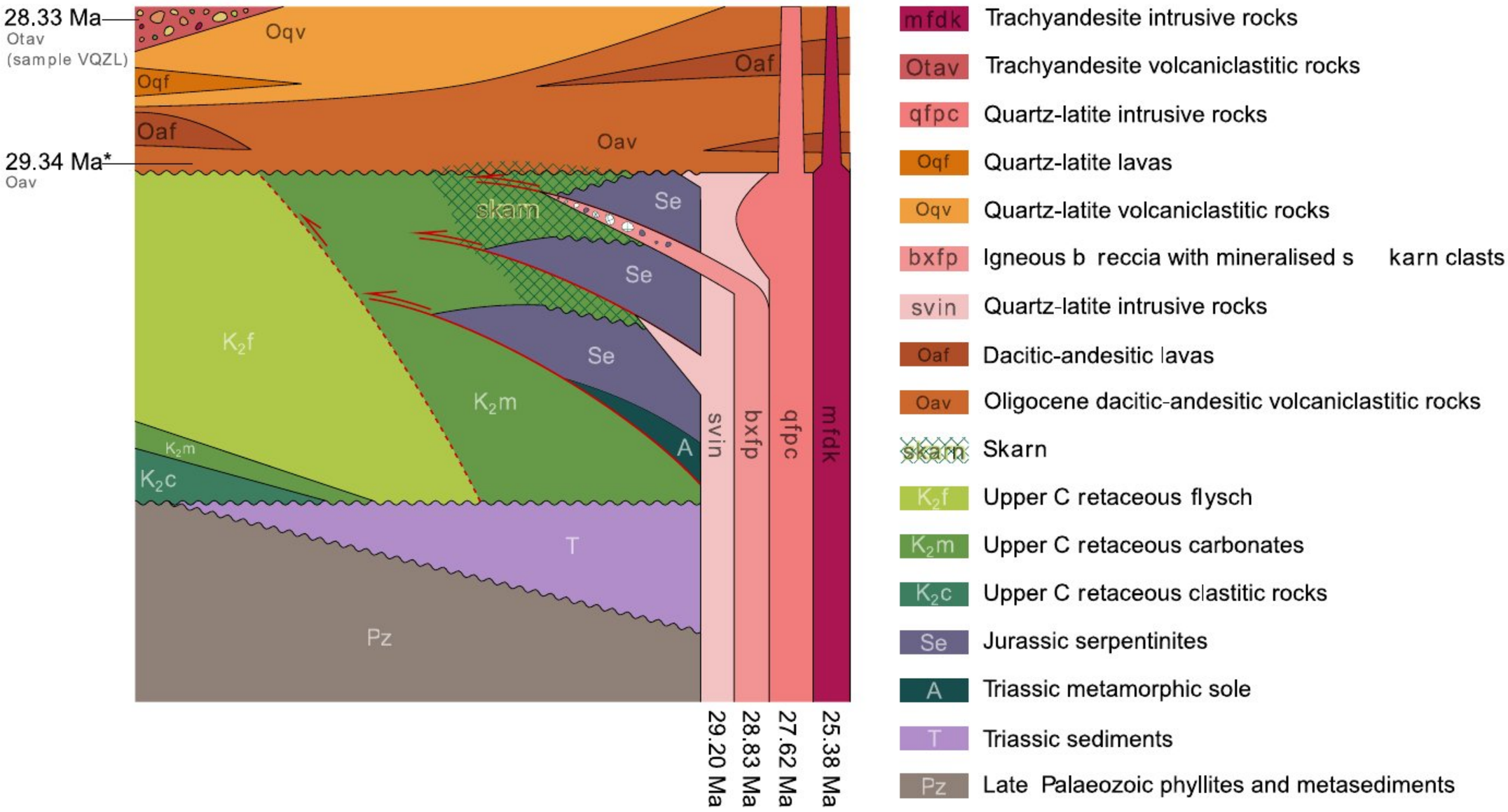

Fig. 8. Schematic depiction of stratigraphic and temporal relationships of main lithological units at Rogozna magmatic. This figure is not to scale and does not include all of the structures observed between the various units. The geochronology in this figure is from this study, and the chronology from the unit marked by an asterisk is from Hoerler et al. (2022). See text for details.

0.03 Ma (Hoerler et al., 2022; sample QFPC1 in this study). Observations from recent drilling campaigns indicate that the groundmass-dominated textures (i.e. QFPP) are commonly found near margins of crowded porphyritic intrusive rocks (i.e. QFPC) or relatively narrow dikes, and it is interpreted that this reflects more rapid cooling of the lower volume, finer grained intrusive bodies. Furthermore, modal and trace element compositions are nearly identical between the two varieties, suggesting a similar genetic history for the two textural end members (Fig. 6). Therefore, the previously reported age of emplacement of the groundmass-dominated quartz-latitic dykes (i.e. QFPP; Hörler, 2017; Hoerler et al., 2022) does not represent a distinctive igneous unit, but rather part of a protracted period of incremental emplacement of quartz-latitic intrusions over 176 ± 43 kyr.

The final period of magmatism at the RMC is represented by the 25.384 ± 0.068 Ma trachyandesitic dike sampled from the Copper Canyon deposit (sample MFDK). Based on field relationships, volcanic rocks of similar compositions exposed further west were previously reported as the youngest constituents of the RMC (NW of Jeleč hill in Fig. 2; e.g. Urošević et al., 1973). We interpret these volcanic rocks to be part of the same pulse of magmatism based on their similar composition, however due to the lack of relative age relationships or high-precision geochronology, we cannot interpret if these volcanic rocks predate, are coeval or postdate the late dikes analyzed in this study. This final pulse of magmatism at the RMC is also broadly synchronous with the regional pulse of shoshonitic magmatism of roughly the same age (e.g., Cvetković et al., 2004).

5.3. Implications for the Development of the Ore Mineral System at the Rogozna magmatic complex

Incorporating these new geochronology data and field observations with previously published information about the alteration and mineralization of the RMC yields a more complex, detailed history of the mineral system responsible for Au-Pb-Zn-Cu mineralization than previously identified (Fig. 9). Previous work interpreted that the initial period of skarn formation at the RMC was associated with the earliest pulse(s) of magmatism (Hoerler et al., 2022). Drill core observations (e.g. ZRSD21136 at the Medenovac deposit, EOKSC1678 at the Šanac deposit) show low-grade metasomatic replacement and mineralization at the base of the volcanic cover, which indicates that the earliest volcanic pulse represents the maximum age of skarn retrogression, previously dated at 29.343 ± 0.03 Ma (Fig. 7; Hoerler et al., 2022). The presence of mineralized skarn clasts within the 28.833 ± 0.043 Ma igneous breccia sample confirms this interpretation, as initial skarn formation must have occurred prior to the crystallization of this breccia's groundmass (Figs. 7 and 9). Therefore, initial skarn formation at Medenovac must have taken place between 29.343 ± 0.03 and 28.833 ± 0.043 Ma.

Previous work indicated that the timing of Po + Ccp + Sp + Apy mineralization hosted in the skarns of the RMC overlaps with the period of incremental emplacement of the crowded porphyry unit between 27.759 ± 0.013 and 27.619 ± 0.01 Ma at the Gradina deposit, based on the fact that the earlier dike is mineralized whereas the later, groundmass dominated dike is unmineralized (Burkhard, 2017; Hoerler et al., 2022). In this interpretation, the incremental emplacement of the quartz latite "crowded porphyry" unit is responsible for much of the diverse metal enrichments found within the RMC. However, the skarn clasts in the igneous breccia sample BXFP host Ccp + Sp mineralization, and therefore Au + Cu + Zn mineralization must have occurred prior to 28.833 ± 0.043 Ma, at least at the Medenovac deposit of the RMC. Furthermore, the mineral assemblages at Medenovac and southern deposits (i.e., Gradina, Copper Canyon, and Šanac deposits) show contrasting oxidation states of mineralization, with the former including hematite, and the latter pyrrhotite. Therefore, there must have been an earlier pulse of oxidized mineralization, indicating that either initial skarn formation was associated with mineralization, or there was a separate hydrothermal event or set of events between 28.833 ± 0.043 and 27.759 ± 0.013 Ma which formed relatively oxidized Au-Cu + Zn mineralization.

This early mineralization event was followed by a period of mineralization and alteration associated with the intrusion of the "crowded

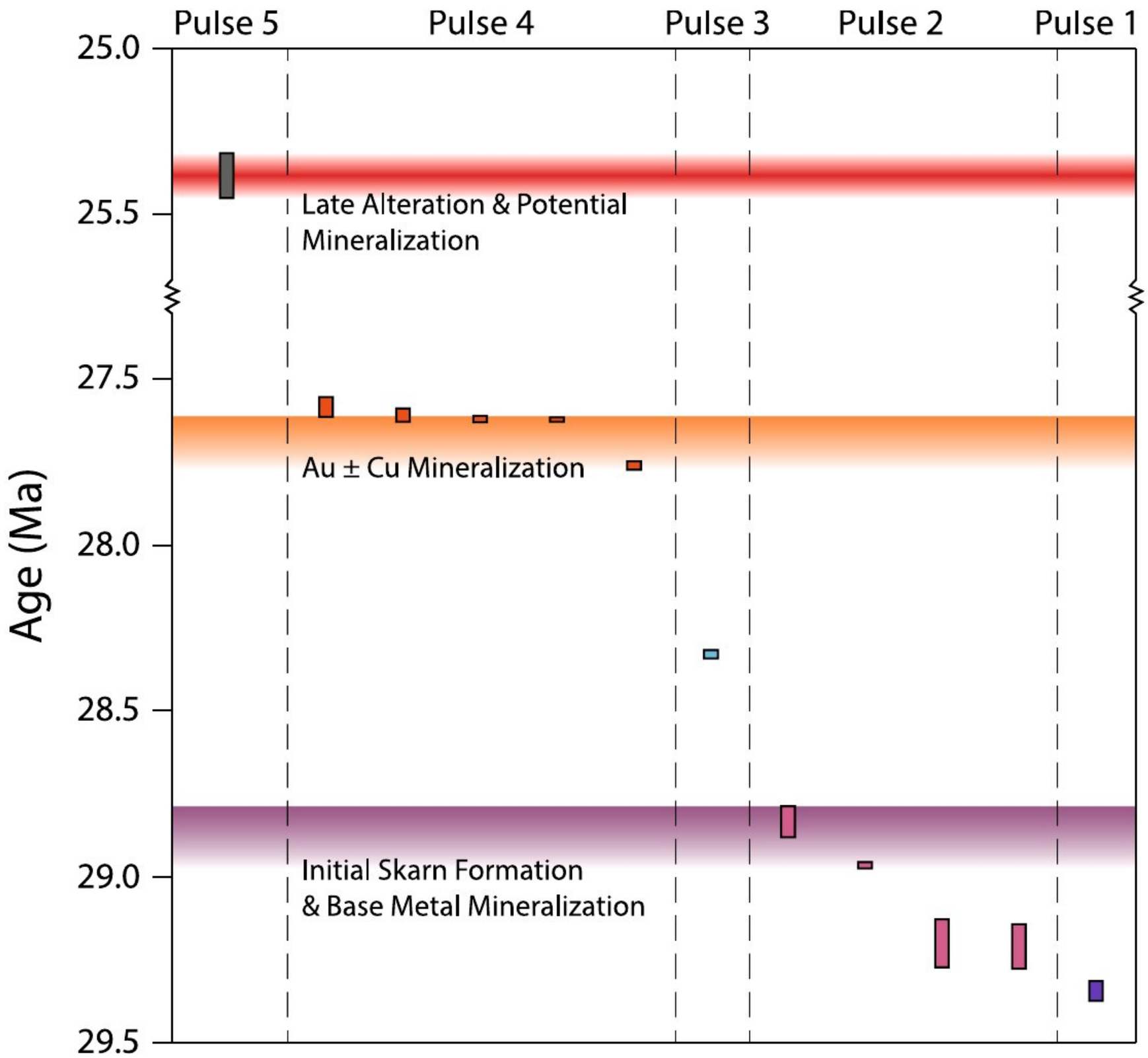

Fig. 9. Interpreted geologic development of the Rogozna magmatic complex and associated mineralization based on high-precision geochronology from Hoerler et al. (2022) and this study, highlighting the interpreted periods of magmatism, alteration and mineralization observed in the deposit. All data plotted on this figure are CA-ID-TIMS U-Pb zircon age interpretations, with the height of each bar representing the 2σ analytical uncertainty of that interpretation. See text for discussion.

porphyry" dikes, wherein mineralization associated with reduced fluids likely began around 27.759 ± 0.013 Ma and terminated with the final stages of its incremental assembly at 27.58 ± 0.03 Ma (Hoerler et al., 2022). Rather, we suggest that this period of alteration and mineralization was episodic, with the formation and collapse of the mineralizing hydrothermal network depending upon the magma injection rate into the subvolcanic region, based on its protracted emplacement and association with texturally diverse dike swarm. This interpretation is similar to deposit models wherein small volume dike swarms incrementally formed mineralizing hydrothermal systems, which allowed for episodic metal enrichment to reach economic levels (e.g., Carten et al., 1988; Betsi and Lentz, 2011; Gaynor et al., 2019a).

Finally, although the age spectra from the early, altered quartz-latite intrusions are quite complex, these complexities provide new insights about alteration and potentially mineralization at the deposit (samples SVIN-1 and SVIN-2; Fig. 7). Due to the lack of overlap and the presence of normal discordance within the younger populations in both samples, they likely represent periods of either Pb-loss or zircon recrystallization. Although chemical abrasion is largely highly effective at mitigating Pb-loss, recent examples from ore forming systems suggest that high-temperature fluid alteration may impose Pb-loss and/or potentially cause recrystallization (e.g., Gaynor et al., 2019a; Rosera et al., 2021; Ouyang et al., 2023). Partial resetting or recrystallization of the U-Pb systematics creates a two-component mixing solution, with the volumetric percentages of mixing dictating the resulting date of the whole grain (e.g., Gaynor et al., 2022). In this situation, the date of an altered zircon crystal may not directly represent the period of alteration, but a suite of such grains will indicate a period of resetting at least as young as the youngest period. Recent work has also shown that in other skarn forming systems, periods of later mineralization were responsible for significant alteration of early mineralizing intrusions, yielding high-precision zircon dates in the timeframe of later high-temperature mineralization events, although those late high temperature events were only revealed within high-precision geochronology and not through field relationships (Ouyang et al., 2023). Therefore, we suggest that the RMC may have undergone a period of alteration and potentially mineralization after 25 Ma, and potentially also during the period of trachyandesite magmatism at 25.384 ± 0.068 Ma.

These observations and interpretations suggest that mineralization at the RMC was not a two-stage process of skarn formation followed by epithermal and base metal mineralization (e.g., Hoerler et al., 2022). Instead, these new data reveal that repeated intrusion of compositionally diverse magmas into the subvolcanic level of the RMC facilitated a repetitive cycle of the growth and collapse of discrete hydrothermal systems, which had different roles in the alteration and mineralization of the RMC. This fits into a growing body of research that shows that many mineral systems are assembled through a protracted magmatic history with different, discrete bodies of magma (e.g., de Ronde et al., 2011; Gaynor et al., 2019a; Large et al., 2021; Lee et al., 2021; Tomlinson et al., 2021; Gaynor et al., 2023). The recognition of the complicated temporal assembly of this deposit required detailed high-precision CA-ID-TIMS U-Pb zircon geochronology to resolve the sub 100 kyr processes

related to mineralization. While this kind of workflow is far more time consuming than alternative in-situ techniques, the advantages in both precision and accuracy are necessary to build accurate models for mineral systems when directly compared to less precise in-situ techniques (e.g., Chelle-Michou et al., 2014; Large et al., 2020; Hoerler et al., 2022).

The approximately 4 Myr duration of hydrothermal-magmatic activity at the RMC resulted in a series of compositionally variable magmas and a series of discrete deposits with varying metal enrichments. While compilations of the total duration of mineralization of many ore deposits have indicated that there is a positive correlation between total duration and deposit endowment, most porphyry deposits yield total durations of less than 1 Myr (e.g., Chiaradia, 2020). The 176 ± 43 kyr cyclical hydrothermal-magmatic activity associated with the emplacement of the texturally variable quartz latite fits within the commonly observed duration of many porphyry deposits. However, the overall duration of hydrothermal-magmatic activity at the RMC is over an order of magnitude more protracted and created ore deposits associated with highly compositionally variable hydrothermal systems. We suggest that the overall enrichment of metals within the upper crustal RMC region was due to the approximately 4 Myr period of periodic formation of hydrothermal-magmatic systems, which allowed for separate periods of mineralization with different metal affiliations and redox states throughout its history. During this period, it's possible the region underwent erosion and unroofing, allowing for different observed expressions of mineralization due to changes in pressure at the current exposure level. However, we suggest that the poly-metallic characteristics of the ore deposits at the RMC was largely driven through shifts in magma genesis within the long-lived magmatic center throughout its lifespan, based on the compositional shifts in the magmas associated with alteration and mineralization over its 4 Myr history. While porphyry mineral systems may be comparably short-lived, more protracted magmatism can allow for a diverse suite of ore deposits at the district scale.

6. Conclusions

Field relationships, textural analyses, and high-precision CA-ID-TIMS U-Pb zircon geochronology reveals a more complicated magmatic and mineralization history of the Rogozna ore deposits than previously interpreted, and was assembled through five discrete magmatic periods, variably associated with hydrothermal alteration and mineralization. The onset of intrusive magmatism was at approximately 29.2 Ma, postdating the onset of volcanism within the field at approximately 29.34 Ma. Approximately 29.2 and 28.883 ± 0.047 Ma marks the initial period of skarn formation and oxidized Au-Zn mineralization, marked by the inclusion of hematite-bearing mineralized skarn clasts within a subsurface breccia with igneous groundmass. This predates the onset of the texturally composite quartz-latite unit between approximately 27.76–27.61 Ma, which was associated with significant reduced (i.e. pyrrhotite-bearing) Cu-Au mineralization within the RMC, and concludes with a final pulse of barren quartz-latite at approximately 27.58 Ma. Finally, a late pulse of trachyandesite dikes at 25.384 ± 0.068 Ma marks the end of Oligocene magmatism at the deposit. Altogether, these results serve as an excellent example of the protracted, episodic evolution of a mineral system, wherein multiple pulses of magmatism sequentially alter and mineralize upper crustal rocks to form an ore deposit.

Declaration of Competing Interest

The authors declare that they have no known competing financial interests or personal relationships that could have appeared to influence the work reported in this paper.

Data availability

The data used in the manuscript are all provided with the manuscript

Acknowledgements

This research was supported by the Swiss National Science Foundation project No. 200020_182007 to U.S., contract on realization and financing of scientific research of SRI in 2022", Nr. 451-03-68/2022-14/200126, and Zlatna Reka Resources. Mineral separation work was supported by Mélissa Ruiz. Assay data for Figure 6 was provided courtesy of Zlatna Reka Resources. The authors gratefully acknowledge the fruitful discussions with Jon Hronsky which helped improve this article. Thanks to Editor-in-Chief Huayong Chen for the handling of this manuscript, and to two anonymous reviewers and Fernando Corfu for thorough, constructive reviews of the manuscript.

Appendix A. Supplementary data

Supplementary data to this article can be found online at https://doi.org/10.1016/j.oregeorev.2023.105775.

References

Andrić, N., Vogt, K., Matenco, L., Cvetković, V., Cloetingh, S., Gerya, T., 2018. Variability of Orogenic Magmatism during Mediterranean-Style Continental Collisions: A Numerical Modelling Approach. Gondwanan Res. 56, 119–134.

Antoine, C., Spikings, R.A., Miletic, D., Marsh, J.S., Gaynor, S.P., Schaltegger, U., 2022. ^{39}Ar-^{40}Ar Geochronology of the Drakensberg Continental Flood basalts: Understanding Large Argon Isotopic Variations in Mafic Groundmass and Plagioclase Size Fractions. Chem. Geol. 610, 121086 https://doi.org/10.1016/j.chemgeo.2022.121086.

Baker, T., 2019. Gold ± Copper Endowment and Deposit Diversity in the Western Tethyan Magmatic Belt, Southeast Europe: Implications for Exploration. Econ. Geol. 114, 1237–1250.

Barboni, M., Schoene, B., 2014. Short eruption window revealed by absolute crystal growth rates in a granitic magma. Nat. Geosci. 7, 524–528.

Betsi, T.B., Lentz, D., 2011. Petrochemistry of subvolcanic dike swarms associated with the Golden Revenue Au-Cu and Stoddart Mo-Cu ± W mineralizations (Dawson Range, Yukon Territory, Canada) and implications for ore genesis. Ore Geol. Rev. 39, 134–163.

Bogdanović, P., 1982. Explanatory book for sheet Kosovska Mitrovica: OGK 1:100 000. Federal Geological Survey, Belgrade.

Borojević Šoštarić, S., Palinkaš, A.L., Neubauer, F., Cvetković, V., Bernroider, M., Genser, J., 2014. The origin and age of the metamorphic sole from the Rogozna Mts., Western Vardar Belt: New evidence for the one-ocean model for the Balkan ophiolites. Lithos 192–195, 39–55. https://doi.org/10.1016/j.lithos.2014.01.011.

Borojević-Šoštarić, S., Cvetković, V., Neubauer, F., Palinkaš, L.A., Bernroider, M., Genser, J., 2012, Oligocene shoshonitic rocks of the Rogozna Mts. (Central Balkan Peninsula): Evidence of petrogenetic links to the formation of Pb–Zn–Ag ore deposits: Lithos, 148, 176-195, doi: 10.1016/j.lithos.2012.05.028 .

Borojević-Šoštarić, S., Palinkaš, L.A., Topa, D., Spangenberg, J.E., Prochaska, W., 2011. Silver–base metal epithermal vein and listwaenite types of deposit Crnac, Rogozna Mts., Kosovo. Part i: Ore Mineral Geochemistry and Sulfur Isotope Study. Ore Geol. Rev. 40, 65–80. https://doi.org/10.1016/j.oregeorev.2011.05.002.

Borojević-Šoštarić, S., Palinkaš, L.A., Neubauer, F., Hurai, V., Cvetković, V., Roller-Lutz, T., Mandić, M., Genser, J., 2013. Silver-base metal epithermal vein and listwanite hosted deposit Crnac, Rogozna Mts., Kosovo, part II: A link between magmatic rocks and epithermal mineralization. Ore Geol. Rev. 50, 98–117. https://doi.org/10.1016/j.oregeorev.2012.10.005.

Bowring, J.F., McLean, N.M., Bowring, S.A., 2011. Engineering cyber infrastructure for U-Pb geochronology: tripoli and U-Pb_Redux. Geochem. Geophys. Geosyst. 12, 19–p.

Budinov, Z.D., Yonezu, K., Tindell, T., Gabo-Ratio, J.A., Milutinović, S., Boyce, A.J., Watanabe, K., 2015. Copper-Gold Skarn Mineralization at the Karavansalija Ore Zone, Rogozna Mountain, Southwestern Serbia. Resource Geol. 65, 328–344. https://doi.org/10.1111/rge.12075.

Buret, Y., Wotzlaw, J.F., Roozen, S., Guillong, M., von Quadt, A., Heinrich, C.A., 2017. Zircon petrochronological evidence for a plutonic-volcanic connection in porphyry copper deposits. Geology 45, 623–626.

Burkhard, R., 2017. Style, relative timing and precipitation conditions of the Au mineralisation at Karavansalija ore zone, Rogozna Mts., Serbia. ETH Zürich. MSc thesis.

Carten, R.B., Geraghty, E.P., Walker, B.M., Shannon, J.R., 1988. Cyclical development of igneous features and their relationship to high-temperature hydrothermal features in the Henderson porphyry molybdenum deposit, Colorado. Econ. Geol. 83, 266–296.

Cathles, L.M., Erendi, A.H.J., Barrie, T., 1997. How long can a hydrothermal system be sustained by a single intrusive event? Econ. Geol. 92, 766–771.

Chelle-Michou, C., Chiaradia, M., Ovtcharova, M., Ulianov, A., Wotzlaw, J.F., 2014. Zircon petrochronology reveals the temporal link between porphyry systems and the

magmatic evolution of their hidden plutonic roots (the Eocene Coroccohuayco deposit, Peru). Lithos 198, 129–140.
Chiaradia, M., 2020. Gold endowments of porphyry deposits controlled by precipitation efficiency. Nat. Commun. 11, 248.
Chiaradia, M., Merino, D., Spikings, R., 2009. Rapid transition to long-lived deep crustal magmatic maturation and the formation of giant porphyry-related mineralization (Yanacocha, Peru). Earth Planet. Sci. Lett. 288, 505–515.
Condon, D.J., Schoene, B., McLean, N.M., Bowring, S.A., Parrish, R.R., 2015. Metrology and traceability of U-Pb isotope dilution geochronology (EARTHTIME Tracer Calibration Part I). Geochim. Cosmochim. Acta 164, 464–480.
Correa, K.J., Rabbia, O.M., Hernández, L.B., Selby, D., Astengo, M., 2016. The Timing of Magmatism and Ore Formation in the El Abra Porphyry Copper Deposit, Northern Chile: Implications for Long-Lived Multiple-Event Magmatic-Hydorthermal Porphyry Systems. Econ. Geol. 111, 1–28.
Cvetković, V., Prelević, D., Downes, H., Jovanović, M., Vaselli, O., Pécskay, Z., 2004. Origin and Geodynamic Significance of Tertiary Postcollisional Basaltic Magmatism in Serbia v. 73, 161–186.
de Ronde, C.E.J., Massoth, G.J., Butterfield, D.A., Christenson, B.W., Ishibashi, J., Ditchburn, R.G., Hannington, M.D., Brathwaite, R.L., Lupton, J.E., Kamenetsky, V.S., Graham, I.J., Zellmer, G.F., Dziak, R.P., Embley, R.W., Dekov, V.M., Munnik, F., Lahr, J., Evans, L.J., Takai, K., 2011. Submarine hydrothermal activity and gold-rich mineralization at Brothers Volcano, Kermadec Arc, New Zealand. Mineralium Deposita 46, 541–584.
Dimitrijević, M.D., 1997. Geology of Yugoslavia. Geological Institute GEMINI, Belgrade.
Dungan, M.A., Wulff, A., Thompson, R., 2001. Eruptive Stratigraphy of the Tatara-San Pedro Complex, 36°S, Southern Volcanic Zone, Chilean Andes: Reconstruction Method and Implications for Magma Evolution at Long-lived Arc Volcanic Centers. J. Petrol. 42, 555–626.
Feely, M., Costanzo, A., Gaynor, S.P., Selby, D., McNulty, E., 2020. A review of molybdenite, and fluorite mineralization in Caledonian granite basement, western Ireland, incorporating new field and fluid inclusion studies, and Re-Os and U-Pb geochronology. Lithos 354–355. https://doi.org/10.1016/j.lithos.2019.105267.
Gallhofer, D., von Quadt, A., Peytcheva, I., Schmid, S.M., Heinrich, C.A., 2015. Tectonic, Magmatic, and Metallogenic Evolution of the Late Cretaceous Arc in the Carpathian-Balkan Orogen 34, 1813–1836.
Gaynor, S.P., Coleman, D.S., Rosera, J.M., Tappa, M.J., 2019b. Geochronology of a Bouguer Gravity Low. J. Geophys. Res. Solid Earth 124, 2457–2468. https://doi.org/10.1029/2018JB015923.
Gaynor, S.P., Rosera, J.M., Coleman, D.S., 2019a. Intrusive history of the Oligocene porphyry molybdenum deposit, New Mexico. Geosphere 15, 548–575.
Gaynor, S.P., Ruiz, M., Schaltegger, U., 2022. The importance of high-precision in the evaluation of U-Pb zircon age spectra. Chem. Geol. 603, 120913.
Gaynor, S.P., Rosera, J.M., Coleman, D.S., 2023. Genesis of the Questa Mo Porphyry Deposit and Nearby Polymetallic Mineralization, New Mexico, USA. Econ. Geol. 118, 1319–1339. https://doi.org/10.5382/econgeo.5011.
Groves, D.I., Santosh, M., Müller, D., Zhang, L., Deng, J., Yang, L.Q., Wang, Q.F., 2022. Mineral systems: Their advantages in terms of developing holistic genetic models and for target generation in global mineral exploration. Geosyst. Geoenviron. 1, 100001.
Heinrich, C.A., Neubauer, F., 2002. Cu–Au(–Pb–Zn–Ag) metallogeny of the Alpine–Balkan–Carpathian–Dinaride geodynamic province: introduction. Miner. Deposita 37, 533–540. https://doi.org/10.1007/s00126-002-0271-x.
Hiess, J., Condon, D.J., McLean, N., Noble, S.R., 2012. $^{238}U/^{235}U$ systematics in terrestrial uranium-bearing minerals. Science 335, 1610–1614.
Hoerler, J., Von Quadt, A., Burkhard, R., Peytcheva, I., Cvetkovic, V., Baker T., 2022, The Karavansalija Mineralized Center at the Rogozna Mountains in SW Serbia: Magma Evolution and Time Relationship of Intrusive Events and Skarn Au ± Cu–Pb–Zn Mineralization: Frontiers in Earth Science, v. 9, 798701, doi: 10.3389/feart.2021.798701.
Hörler, J., 2017. The Karavansalija ore zone at Rogozna Mt. in southwestern Serbia: Magma evolution and time relationship of intrusive events, skarn mineralization and overlying volcanics. ETH Zürich. MSc thesis.
Janković, S., 1990. Rudna ležišta Srbije (Ore deposits of Serbia). Faculty of Mining and Geology, Belgrade. (760. In: Serbian with English summary).
Janković, S., 1997. The Carpatho-Balkanides and adjacent area: a sector of the Tethyan Eurasian metallogenic belt. Miner. Deposita 32, 426–433.
Janković, S., 1995, The principal metallogenetic features of the Kopaonik District: In Karamata, S. and Janković, S. (eds.), Proceedings of the International Symposium "Geology and Metallogeny of the Dinarides and the Vardar Zone", Academy of Science and Art of Republika Srpska, Banja Luka, v. 1, p. 79–102.
Jelenković, R., Kostić, A., Životić, D., Ercegovac, M., 2008. Mineral resources of Serbia. Geol. Carpath. 59 (4), 345–361.
Karamata, S., 2006. The geological development of the Balkan Peninsula related to the approach, collision and compression of Gondwanan and Eurasian units: Geological Society. London, Special Publications 260, 155–178.
Karamata, S., Krstić, B., Stojanov, R., 1992, Terranes from the Adriatic to the Moesian Massif in the Central Part of the Balkan Peninsula: Abstracts supplement of the "ALCAPA Symposium, Graz 1992", v. 2, p. 36.
Karamata, S., Pécskay, Z., Knežević, V., Memović, E., 1994. Origin and age of Rogozna (Central Serbia) volcanics in the light of new isotopic data: Bulletin de l'Académie serbe des sciences et des arts, Classe des sciences mathématiques et naturelles. Sciences Mathématiques 108, 35, 41–46.
Krogh, T.E., 1973. A low-contamination method for hydrothermal decomposition of zircon and extraction of U and Pb for isotopic age determinations. Geochim. Cosmochim. Acta 37, 485–494.
Large, S.J.E., Buret, Y., Wotzlaw, J.F., Karakas, O., Guillong, M., von Quadt, A., Heinrich, C.A., 2021. Copper-mineralised porphyries sample the evolution of a large-volume silicic magma reservoir from rapid assembly to solidification. Earth Planet. Sci. Lett. https://doi.org/10.1016/j.epsl.2021.116877.
Large, S.J., Wotzlaw, J.F., Guillong, M., Quadt, A.V., Heinrich, C.A., 2020. Resolving the timescales of magmatic and hydrothermal processes associated with porphyry deposit formation using zircon U-Pb petrochronology. Geochronology 2, 209–230.
Lee, W.S., Kontak, D.J., Richards, J.P., Barresi, T., Creaser, R.A., 2021. Superimposed Porphyry Systems in the Dawson Range no. 24, 29–48.
Li, Y., Selby, D., Condon, D., Tapster, S., 2017. Cyclic magmatic-hydrothermal evolution in porphyry systems: high-precision U-Pb and Re-Os geochronology constraints on the Tibetan Qulong porphyry Cu-Mo deposit. Econ. Geol. 112, 1419–1440.
Mattinson, J.M., 2005. Zircon U-Pb chemical abrasion ("CA-TIMS") method: combined annealing and multi-step partial dissolution analysis for improved precision and accuracy of zircon ages. Chem. Geol. 220, 47–66.
McLean, N.M., Bowring, J.F., Bowring, S.A., 2011. An algorithm for U-Pb isotope dilution data reduction and uncertainty propagation. Geochem. Geophys. Geosyst. https://doi.org/10.1029/2010GC003479.
Miletić, G., Milutinović, S., Rakić, N., 1998. Synthesis of the geologic investigation of the Belo Brdo ore field: Geozavod-IMS. Belgrade 1–19 in Serbian.
Moritz, R., Noverraz, C., Márton, I., Marchev, P., Spikings, R., Fontignie, D., Spangenberg, J.E., Vennemann, T., Kolev, K., Hasson, S., 2014. Sedimentary-rock-hosted Epithermal Systems of the Tertiary Eastern Rhodopes, Bulgaria: New Constraints from the Stremtsi Gold Prospect. Geol. Soc. Lond. Spec. Publ. 402, 207–230.
Moritz, R., Rezeau, H., Ovtcharova, M., Tayan, R., Melkonyan, R., Hovakimyan, S., Ramazanov, V., Selby, D., Ulianov, A., Chiaradia, M., Putlitz, B., 2016. Long-lived, stationary magmatism and pulsed porphyry systems during Tethyan subduction to post-collision evolution in the southernmost Lesser Caucasus, Armenia and Nakhitchevan. Gondwana Res. 37, 465–503.
Mundil, R., Ludwig, K.R., Metcalf, I., Renne, P.R., 2004. Age and timing of the Permian mass extinctions: U/Pb dating of closed-system zircons. Science 305, 669–673.
Ouyang, H., Gaynor, S.P., Hu, R., Selby, D., Mao, J., Shu, Q., Li, C., 2023. High-precision geochronology of the Xiaojiayingzi Mo skarn deposit: Implications for prolonged and episodic and hydrothermal pulses. Econ. Geol. 118, 485–507.
Ovtcharova, M., Goudemand, N., Hammer, Ø., Guodun, K., Cordey, F., Galfetti, T., Schaltegger, U., Bucher, H., 2015. Developing a strategy for accurate definition of a geological boundary through radio-isotopic and biochronological dating: The Early-Middle Triassic boundary (South China). Earth Sci. Rev. 146, 65–76.
Prelević, D., Foley, S.F., Romer, R.L., Cvetković, V., Downes, H., 2005. Tertiary Ultrapotassic Volcanism in Serbia: Constraints on Petrogenesis and Mantle Source Characteristics. J. Petrol. 46 (7), 1443–1487.
Rosera, J.M., Gaynor, S.P., Coleman, D.S., 2021. Spatio-temporal shifts in magmatism and mineralization in northern Colorado beginning in the late Eocene. Econ. Geol. 116, 987–1010.
Schaltegger, U., Brack, P., Ovtcharova, M., Peytcheva, I., Schoene, B., Stracke, A., Marocchi, M., Bargossi, G.M., 2009. Zircon and titanite recording 1.5 million years of magma accretion, crystallization and initial cooling in a composite pluton (southern Adamello batholith, northern Italy). Earth Planet. Sci. Lett. 286, 208–218.
Schaltegger, U., Ovtcharova, M., Gaynor, S.P., Schoene, B., Wotlzaw, J.F., Davies, J.H.F. L., Farina, F., Greber, N., Szymanowski, D., Chelle-Michou, C., 2021. Long-Term Repeatability and Interlaboratory Reproducibility of High-Precision ID-TIMS U-Pb Geochronology. J. Anal. Atom. Spectr. https://doi.org/10.1039/d1ja00116g.
Schefer, S., 2010. Tectono-metamorphic and magmatic evolution of the Internal Dinarides (Kopaonik area, southern Serbia) and its significance for the geodynamic evolution of the Balkan Peninsula. University of Basel, p. 230 pp.. PhD thesis.
Schmid, S.M., Bernoulli, D., Fügenschuh, B., Matenco, L., Schefer, S., Schuster, R., Tischler, M., Ustaszewski, K., 2008. The Alpine-Carpathian-Dinaridic orogenic system: correlation and evolution of tectonic units. Swiss J. Geosci. 101, 139–183.
Schmid, S.M., Fügenschuh, B., Kounov, A., Matenco, L., Nievergelt, P., Oberhänsli, R., Pleuger, J., Schefer, S., Schuster, R., Tomljenović, B., Ustaszewski, K., van Hinsbergen, D.J.J., 2020. Tectonic units of the Alpine collision zone between Eastern Alps and western Turkey. Gondw. Res. 78, 308–374. https://doi.org/10.1016/j.gr.2019.07.005.
Schoene, B., Crowley, J.L., Condon, D.J., Schmitz, M.D., Bowring, S.A., 2006. Rassessing the uranium decay constants for geochronology using ID-TIMS U-Pb data. Geochim. Cosmochim. Acta 70, 426–445.
Schöpa, A., Annen, C., Dilles, J.H., Sparks, R.S.J., Blundy, J.D., 2017. Magma Emplacement Rates and Porphyry Copper Deposits: Thermal Modeling of the Yerington Batholith, Nevada. Econ. Geol. 112, 1653–1672.
Selby, D., Creaser, R.A., 2001. Re-Os geochronology and systematics in molybdenite from the Endako porphyry molybdenum deposit, British Columbia, Canada. Econ. Geol. 96, 197–204.
Serafimovski, T., Stefanova, V., Volkov, A.V., 2010. Dwarf copper-gold porphyry deposits of the Buchim-Damjan-Borov Dol ore district, Republic of Macedonia (FYROM). Geol. Ore Deposits 52, 179–195.
Sillitoe, R.H., 2010. Porphyry copper systems. Econ. Geol. 105, 3–41.
Tapster, S., Condon, D.J., Naden, J., Noble, S.R., Petterson, M.G., Roberts, N.M.W., Saunders, A.D., Smith, D.J., 2016. Rapid thermal rejuvenation of high-crystallinity magma linked to porphyry copper deposit formation; evidence from the Koloua Porphyry Prospect, Solomon Islands. Earth Planet. Sci. Lett. 442, 206–217.
Tomlinson, D.H.J., Christiansen, E.H., Keith, J.D., Dorais, J.D., Ganske, R., Fernandez, D., Vetz, N., Sorensen, M., Gibbs, J., 2021. Nature and origin of zoned polymetallic (Pb-Zn-Cu-Ag-Au) veins from the Bingham Canyon porphyry Cu-Au-Mo deposit. Economic Geology, Utah.

Urošević, M., Pavlović, Z., Klisić, M., Brković, T., Malešević, M., Trifunović, S., 1973. Explanatory book for sheet Novi Pazar: OGK 1:100 000. Federal Geological Survey, Belgrade.

Velador, J.M., Heizler, M.T., Campbell, A.R., 2010. Timing of Magmatic Activity and Mineralization and Evidence of a Long-Lived Hydrothermal System in the Fresnillo Silver District, Mexico: Constraints from $^{40}Ar/^{39}Ar$ Geochronology. Econ. Geol. 105, 1335–1349.

Whitney, D.L., Evans, B.W., 2010, Abbreviations for names of rock-forming minerals: American Mineralogist, v. 95, p. 185–187; doi:10.2138/am.2010.3371.

Widmann, P., Davies, J.H.F.L., Schaltegger, U., 2019. Calibrating chemical abrasion: Its effects on zircon crystal structure, chemical composition and U-Pb age. Chem. Geol. 511, 1–10.

Zimmerman, A., Stein, H.J., Hannah, J.L., Koželj, D., Bogdanov, K., Berza, T., 2008. Tectonic configuration of the Apuseni–Banat—Timok–Srednogorie belt, Balkans-South Carpathians, constrained by high precision Re–Os molybdenite ages. Miner. Deposita 43, 1–21.